Journal of Saudi Chemical Society (2017) 21, 205–209

King Saud University

Journal of Saudi Chemical Society

www.ksu.edu.sa
www.sciencedirect.com

ORIGINAL ARTICLE

Highly stable and active Ni-doped ordered mesoporous carbon catalyst on the steam reforming of ethanol application

Josh Y.Z. Chiou, Hsuan-Ying Kung, Chen-Bin Wang *

Department of Chemical and Materials Engineering, Chung Cheng Institute of Technology, National Defense University, Tahsi, Taoyuan 33509, Taiwan, ROC

Received 25 August 2015; revised 19 October 2015; accepted 21 October 2015
Available online 26 October 2015

KEYWORDS

Ordered mesoporous carbon;
Steam reforming of ethanol;
Hydrogen

Abstract A novel one-step direct synthesis of nickel embedded in an ordered mesoporous carbon catalyst (NiOMC) is done in a basic medium of nonaqueous solution by a solvent evaporation-induced self-assembly process. The NiOMC sample is characterized by a variety of analytical and spectroscopy techniques, e.g., N_2 adsorption/desorption isotherm measurement, X-ray diffraction (XRD), transmission electron microscopy (TEM) and temperature-programed reduction (TPR). In this study, the NiOMC catalyst is found to exhibit superior catalytic activity for the steam reforming of ethanol (SRE), showing high hydrogen selectivity and durability. Ethanol can be completely converted at 350 °C over the NiOMC catalyst. Also, the durability of the NiOMC catalyst on the SRE reaction exceeds 100 h at 450 °C, with S_{H2} approaching 65% and S_{CO} of less than 1%.

1. Introduction

The use of a high surface area support is a simple and efficient strategy for improving catalytic performance. Mesoporous materials have attracted considerable attention because of their ordered pore structure, high surface area, large pore volume and chemical inertness. Notable prospective applications are catalysis, sorption, gas sensing, ion exchange, optics and photovoltaics [1–5].

Ethanol is an important candidate as a chemical carrier of hydrogen [6]. Hydrogen production from the steam reforming of ethanol (SRE) has been extensively studied [7]. The performance of SRE over Ni-supported catalysts was reviewed by Vaidya and Rodrigues [8]. The Ni catalyst supported on porous materials was wieldy, when used on the SRE for hydrogen production. Carreno et al. [9] reported that a nickel–carbon catalyst possessed a high activity for ethanol steam reforming. Furthermore, the formation of filamentous carbon under 500 and 600 °C with the increase of reaction time did not lead to the deactivation of the catalyst. Active carbon-supported Ni–Cu bimetallic or Ni/Cu/Pd trimetallic catalysts used on the SRE reaction were reported by Özkan et al. [10], where the highest selectivity of hydrogen was given by the catalyst

* Corresponding author. Tel.: +886 3 3891716; fax: +886 3 3808906.
E-mail address: chenbinwang@gmail.com (C.-B. Wang).
Peer review under responsibility of King Saud University.

Production and hosting by Elsevier

http://dx.doi.org/10.1016/j.jscs.2015.10.006
1319-6103

containing palladium at 450 °C. Metals and metal oxides (Ni, Co, Pt and Rh) supported on carbon nanotubes (CNTs) were studied by Seelam et al. [11], with Ni/CNT and Co/CNT catalysts having better catalytic performance.

In this paper, we present a novel one-step method for synthesizing the nickel embedded in the ordered mesoporous carbon catalyst. The SRE reaction with and without the pre-reduction pretreatment is also studied to investigate the catalytic performance.

2. Experimental

An active catalyst of Ni-doped ordered mesoporous carbon was synthesized by means of a solvent evaporation-induced self-assembly (EISA) process. The molar ratio of resorcinol/HCHO/NaOH/F127/$Ni(NO_3)_2{\cdot}6H_2O$ was 1:3:0.083:0.018:0.12 in this process. For solution A, 1.0 g of resorcinol and 0.03 g of NaOH were dissolved together in 16 g of ethanol, followed by the addition of 2.2 g of 37% formaldehyde under magnetic stirring at room temperature. For solution B, 2.0 g of F127 and 0.6 g of $Ni(NO_3)_2{\cdot}6H_2O$ were dissolved in 12.0 g of ethanol under magnetic stirring at room temperature. Then, solution A was added dropwise to solution B and stirring was maintained for 2 h. The homogeneous solution obtained was poured into a dish to evaporate ethanol at room temperature for 24 h, and then kept in an oven at 100 °C for 24 h. Finally, the as-prepared sample was scraped from the dish and carbonized at 700 °C for 2 h under a nitrogen atmosphere. The catalytic performance of the Ni-doped ordered mesoporous carbon catalyst was compared with (assigned as NiOMC-R400) and without (assigned as NiOMC) the pre-reduction pretreatment at 400 °C for 2 h. The physicochemical properties of the NiOMC catalyst are listed in Table 1.

The BET surface area and pore size distribution of the catalyst were measured by N_2 adsorption–desorption using a Micromeritics ASAP 2010 analyzer. X-ray diffraction (XRD) measurements were performed using a Siemens D5000 diffractometer with Cu $K_{\alpha 1}$ radiation at 40 kV and 30 mA. The microstructure and particle size of the samples were observed using transmission electron microscopy (TEM) with a JEOL JEM-2010 microscope equipped with a field-emission electron source and operated at 200 kV.

The catalytic activity of the SRE reaction was evaluated in a fixed-bed flow reactor. For each run, approximately 100 mg of the catalyst was placed in a 4 mm i.d. quartz tubular reactor and held by a glass-wool plug. The temperature of the reactor was controlled by a heating tape and measured by a thermocouple (1.2 mm i.d.) at the center of the reactor bed. The feed of the reactants (H_2O/EtOH/Ar = 37/3/60 vol%) was controlled by the Ar flow stream through a saturator (maintained at 130 °C) containing EtOH and H_2O. The gas hourly space velocity (GHSV) was maintained at 22,000 h^{-1} and the H_2O/EtOH molar ratio was 13. The SRE activity was carried out at 200–500 °C online by gas chromatography (GC) with columns of Porapak Q and a Molecular Sieve of 5 Å, with two sets of thermal conductivity detectors (TCD) for separation and quantitative analysis. The activity evaluation of all samples depended on the conversion of ethanol (X_{EtOH}), the distribution of products (mol%) and the yield of hydrogen (Y_{H2}, mol H_2/mol EtOH) according to the following equations:

$$X_{EtOH} = (n_{EtOH,\ reacted}/n_{EtOH,\ fed}) \times 100\% \quad (1)$$

$$S_i = \left(n_i/\sum n_i\right) \times 100\% \quad (2)$$

$$Y_{H2} = n_{H2\text{-}out}/n_{EtOH,\ reacted} \quad (3)$$

where n_i is a mole of products and includes H_2.

3. Results and discussion

Fig. 1(a) exhibits the small-angle XRD pattern of the NiOMC catalyst; only one diffraction peak of the (1 1 0) plane of the ordered body-centered cubic meso-structure (space group Im3m) can be observed [12]. The wide-angle XRD pattern in Fig. 1(b) shows a broad peak at $2\theta = 23.4°$ (0 0 2), revealing the presence of graphitic carbon. Ni^{2+} was almost completely reduced to metallic nickel with a face-centered cubic structure (JCPDS-04-0850) during the carbonization process at 700 °C, whereas only a faint signal of NiO species (JCPDS 44-1159) was observed. An average particle size of c. 15 nm was deduced for the Ni particles by means of the Scherrer equation, based on the full-width half-maximum (FWHM) line width of the prominent (1 1 1) peak. The N_2 adsorption/desorption isotherms obtained at 77 K for the NiOMC catalyst (Fig. 1(c)) exhibited the typical type IV isotherms, with signature hysteresis loops revealing the presence of mesoporosity, as also revealed by the BJH pore size distribution (inset of Fig. 1(c)). The textural properties determined for both samples are depicted in Table 1. TPR profile of the NiOMC catalyst is shown in Fig. 1(d). A weak signal around 220 °C was attributed to the reduction of NiO [13]. The ratio of NiO was quantitatively determined from the consumption of hydrogen evident in the TPR trace. The relative area approached 0.08, as also evidenced from the XRD analysis. The other signal at 537 °C was related to the methanation of carbon. A previous study [14] revealed that the reduction of carbonaceous species located at 450–600 °C indicated the methanation of carbonaceous species by H_2.

$$C + 2H_2 \rightarrow CH_4 \quad (4)$$

Further TEM experiments were aimed at directly observing the pore structure of the carbon and the distribution of Ni existing in the NiOMC (Fig. 2(a)) sample. Combined with the corresponding XRD pattern, the ordered cubic

Table 1 Physicochemical property of NiOMC catalyst.

Catalyst	Metal loading (%)[a]	BET surface area (m^2/g)	Pore volume (cm^3/g)	Pore diameter (nm)	d_{Ni} (nm)[b]	
					Fresh	Spent
NiOMC	9.2	156	0.73	3.5	15	23
NiOMC-R400	9.2	118	0.62	3.4	20	32

[a] Measured with ICP-AES.
[b] Calculated with Scherrer's formula.

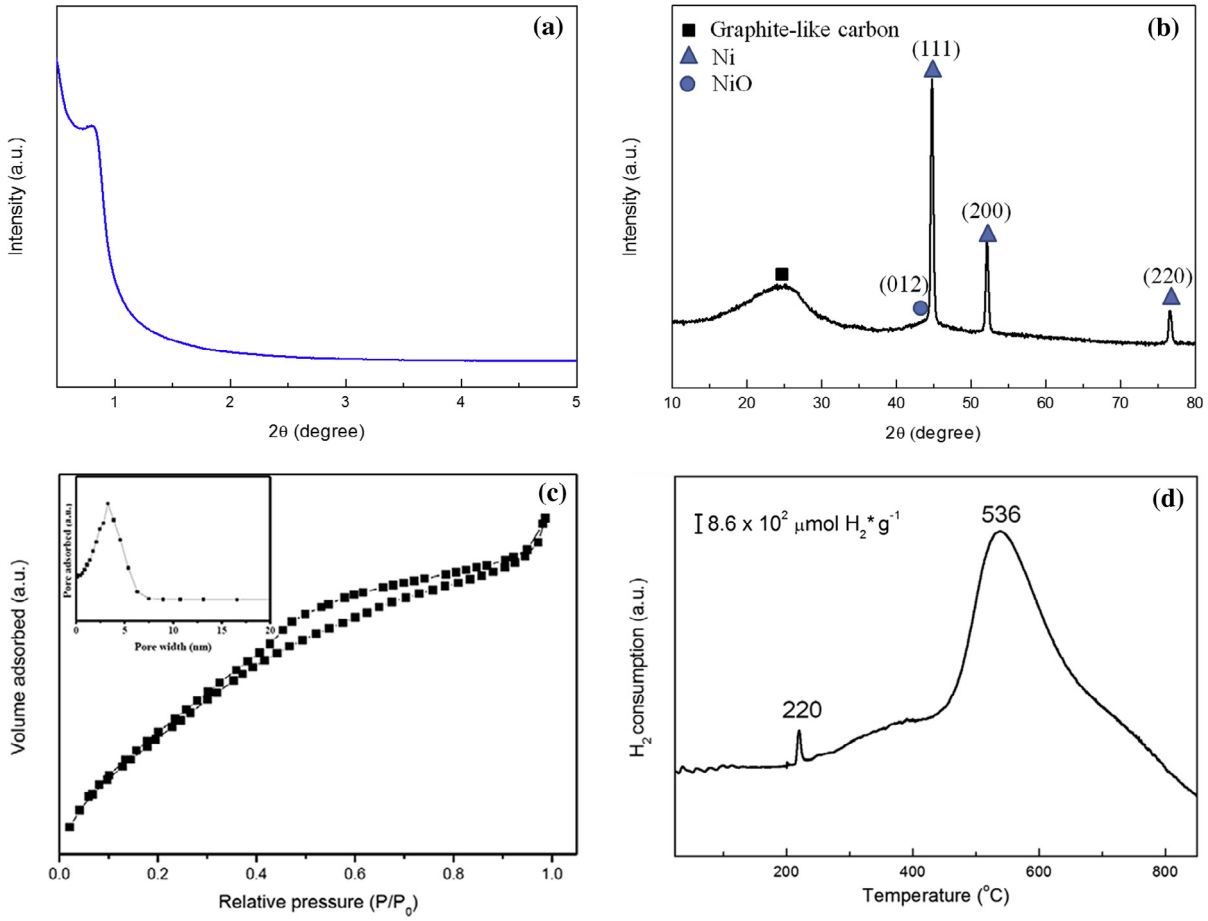

Figure 1 (a) Small angle; (b) wide angle XRD patterns; (c) N_2 adsorption/desorption isotherm and BJH pore size distribution; (d) TPR profile of NiOMC catalyst.

meso-structure was further confirmed from this image. The distribution of dark spots with an average diameter of about 16 nm was identified as the dispersed Ni nanoparticles.

Fig. 3(a) shows the SRE reaction over the NiOMC catalyst to produce hydrogen at different temperatures (T_R). Although the NiOMC catalyst did not pre-reduce pretreatment at 400 °C, results showed the catalytic activity of the NiOMC to be preferential. Ethanol was completely converted at 350 °C. During the SRE reaction, the reforming products, including the reducing gases, i.e., H_2 and CO, might have further reduced the faint NiO into Ni at a temperature lower than 300 °C. So, the nickel metal was the active site in the ethanol reforming process. According to the literatures [15–18], the proposed reforming pathway for the SRE over the NiOMC catalyst is shown in Scheme 1. According to the distribution of products, the predominant reaction at a T_R lower than 300 °C was the dehydrogenation of ethanol to acetaldehyde (Eq. (5)), followed by the decomposition of acetaldehyde to form CH_4 and CO. Above 325 °C, the S_{CO} decreased and S_{CO2} and S_{H2} increased, indicating that the water–gas shift (WGS) reaction (Eq. (6)) had occurred. Also, the rapid S_{H2} and Y_{H2} increase above 350 °C may have been due to the

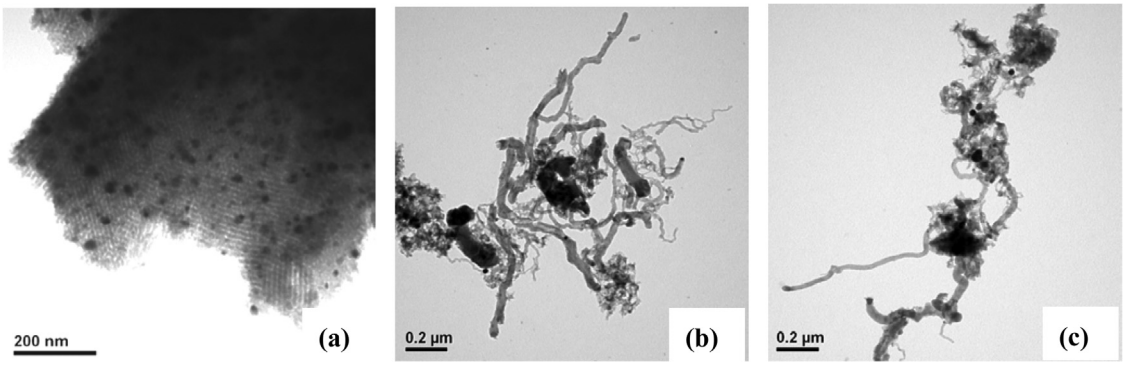

Figure 2 TEM images of (a) fresh NiOMC; (b) spent NiOMC; and (c) spent NiOMC-R400 catalysts.

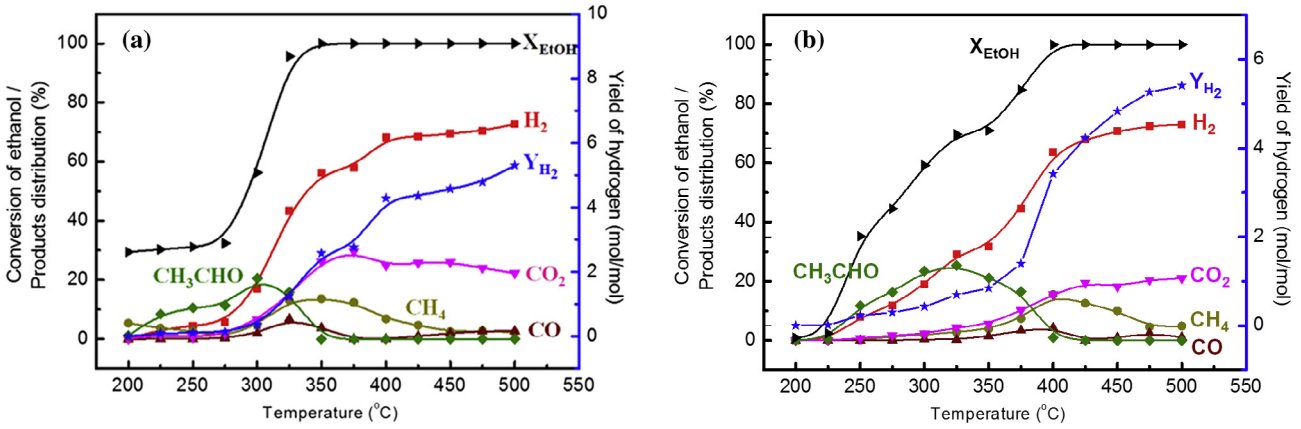

Figure 3 Catalytic performance for SRE reaction over (a) NiOMC and (b) NiOMC-R400 catalysts.

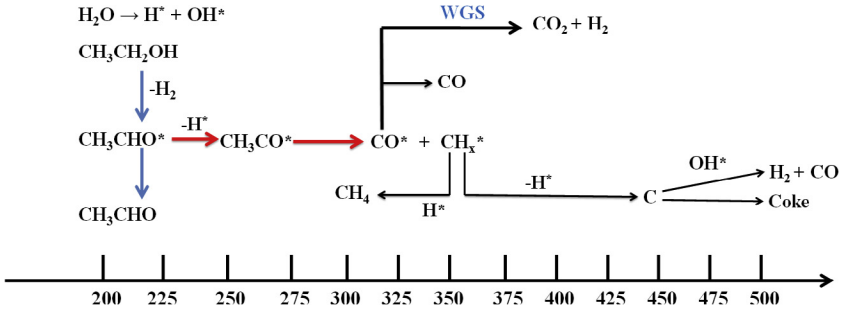

Scheme 1 Reaction pathway for the SRE reaction over NiOMC catalyst.

methane steam reforming reaction (Eq. (7)). As the T_R increased to 450 °C, S_{CO} increased slightly with S_{CO2} decreasing. It was thought that the reverse water–gas shift (RWGS) reaction (Eq. (8)) had occurred. The maximum Y_{H2} was 5.3 at 500 °C.

$$C_2H_5OH \rightarrow CH_3CHO + H_2 \quad (5)$$

$$CO + H_2O \rightarrow CO_2 + H_2 \quad (6)$$

$$CH_4 + H_2O \rightarrow 3H_2 + CO \quad (7)$$

$$CO_2 + H_2 \rightarrow CO + H_2O \quad (8)$$

Prior to the reaction, the NiOMC catalyst was activated by the reduction pretreatment with hydrogen at 400 °C for 2 h, and denoted as NiOMC-R400. The catalytic performance for the SRE reaction over the NiOMC-R400 catalyst is shown in Fig. 3(b). The reaction route of the NiOMC-R400 catalyst was similar to that of the NiOMC catalyst. However, the T_R of the complete conversion of ethanol shifted from 350 °C (NiOMC) to 400 °C (NiOMC-R400). A comparison of both catalysts showed that the dispersed Ni particles were slightly aggregated to 20 nm through the reduction pretreatment and influence of the catalytic activity.

XRD, EA and TEM analyses were used to characterize the NiOMC and NiOMC-R400 catalysts after the SRE reaction. XRD patterns (not shown) revealed that the metallic Ni phase (JCPDS-04-0850) existed on both. Apparently, the faint NiO species reduced to Ni under the H_2-rich environment. The EA measurements showed a carbon deposition on the NiOMC and NiOMC-R400 catalysts of 7.9% and 12%, respectively. TEM images (Fig. 2(b) and (c)) showed that the deposited carbon as nanotubes emerged with the catalyst particles and/or became an amorphous carbon coating on the surface of the catalyst.

One of the main concerns was to develop a stable catalyst for hydrogen production from the SRE reaction. We chose the active NiOMC catalyst for evaluation. Fig. 4 compares

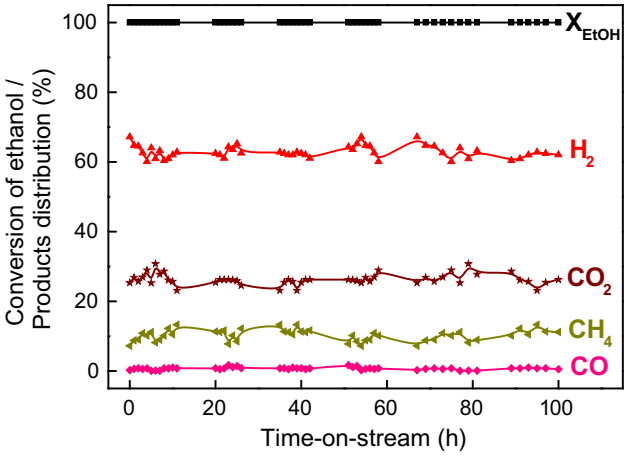

Figure 4 Durability test for the SRE reaction over NiOMC catalyst at 450 °C.

the conversion and distribution of products as a function of time-on-stream (TOS) during the SRE reaction over the NiOMC catalyst under the S/C ratio of 13 at 450 °C. The Ni-doped NiOMC catalyst proved highly stable and active on the SRE reaction. The complete conversion of ethanol was maintained for over 100 h, the S_{H2} approached 65%, the S_{CO} was less than 1%, while the S_{CH4} approached 7–13%.

4. Conclusions

The novel Ni-doped carbon catalyst with an ordered mesoporous structure, high surface area, high catalytic performance and durability on the SRE reaction was designed and facile prepared. Ethanol was completely converted at 350 °C over the NiOMC catalyst. Also, the durability of the NiOMC catalyst on the SRE reaction exceeded 100 h at 450 °C.

Acknowledgement

We are pleased to acknowledge the financial support for this study from the Ministry of Science and Technology of the Republic of China under contract number MOST 104-2119-M-606-001.

References

[1] J.C. Amphlett, S. Leclerc, R.F. Mann, B.A. Peppley, P.R. Roberge, Proceedings of the 33rd Intersociety Energy Conversion Engineering Conference, 1998, pp. 1–7.
[2] V.M. Lisiane, G. Jacobs, H.D. Burtron, B.N. Fabio, Chem. Rev. 112 (2012) 4094–4123.
[3] H.C. Foley, Microporous Mater. 4 (1995) 407–433.
[4] Y. Yamamoto, T. Matsuzaki, K. Ohdan, Y. Okamoto, J. Catal. 161 (1996) 577–586.
[5] A.C. Dillon, K.M. Jones, T.A. Bekkedahl, C.H. Kiang, D.S. Bethune, M.J. Heben, Nature 386 (1997) 377–379.
[6] J. Xu, Z. Luan, M. Hartmann, L. Kevan, Chem. Mater. 11 (1999) 2928–2936.
[7] J.W. Robin, V. Budarin, R. Luque, H.C. James, J.M. Duncan, Chem. Soc. Rev. 38 (2009) 3401–3418.
[8] P.D. Vaidya, A.E. Rodrigues, Chem. Eng. J. 117 (2006) 39–49.
[9] N.L.V. Carreno, I.T.S. Garcia, C.W. Raubach, M. Krolow, C. C.G. Santos, L.F.D. Probst, H.V. Fajardo, J. Power Sources 188 (2009) 527–531.
[10] G. Özkan, S. Gök, G. Özkan, Chem. Eng. J. 171 (2011) 1270–1275.
[11] P.K. Seelam, M. Huuhtanen, A. Sapi, M. Szabo, K. Kordas, E. Turpeinen, G. Toth, R.L. Keiski, Int. J. Hydrogen Energy 35 (2010) 12588–12595.
[12] D. Zhao, Q. Huo, J. Feng, B.F. Chmelka, G.D. Stucky, J. Am. Chem. Soc. 120 (1998) 6024–6036.
[13] H.H. Huang, S.W. Yu, C.L. Chuang, C.B. Wang, Int. J. Hydrogen Energy 39 (2014) 20700–20711.
[14] C.B. Wang, C.C. Lee, J.L. Bi, J.Y. Siang, J.Y. Liu, C.T. Yeh, Catal. Today 146 (2009) 76–81.
[15] M. Ni, D.Y.C. Leung, M.K.H. Leung, Int. J. Hydrogen Energy 32 (2007) 3238–3247.
[16] A. Haryanto, S. Fernando, N. Murali, S. Adhikari, Energy Fuel 19 (2005) 2098–2106.
[17] V. Subramani, C. Song, Catalysis 20 (2007) 65–106.
[18] J.Y.Z. Chiou, C.L. Lee, K.F. Ho, H.H. Huang, S.W. Yu, C.B. Wang, Int. J. Hydrogen Energy 39 (2014) 5653–5662.